X-ray nonlinear optical processes using a self-amplified spontaneous emission free-electron laser

Nina Rohringer and Robin Santra
Argonne National Laboratory, Argonne, Illinois 60439, USA
(Received 24 May 2007; published 27 September 2007)

In contrast to the long-wavelength regime, x-ray nonlinear optical processes are characterized in general by sequential single-photon single-electron interactions. Despite this fact, the sequential absorption of multiple x-ray photons depends on the statistical properties of the radiation field. Treating the x rays generated by a self-amplified spontaneous emission free-electron laser as fully chaotic, a quantum-mechanical analysis of inner-shell two-photon absorption is performed. It is demonstrated that double-core-hole formation via x-ray two-photon absorption is enhanced by chaotic photon statistics. Numerical calculations using rate equations illustrate the impact of field chaoticity on x-ray nonlinear ionization of helium and neon for photon energies near 1 keV. In the case of neon, processes are discussed that involve up to seven photons. Assuming an x-ray coherence time of 2.6 fs, double-core-hole formation in neon is found to be statistically enhanced by about 30% at an intensity of 10^{16} W/cm^2.

DOI: 10.1103/PhysRevA.76.033416 PACS number(s): 32.80.Rm, 32.80.Fb, 42.50.Ar, 41.60.Cr

I. INTRODUCTION

Three x-ray free-electron lasers (FELs) [1,2] are currently under construction: LCLS at the Stanford Linear Accelerator Center [3], the Japanese SCSS at SPring-8 [4], and the European XFEL project at DESY in Hamburg [5]. These new facilities will soon make it possible to explore new frontiers in atomic physics, femtochemistry, materials science, and molecular biology [6–14]. X-ray FELs, with peak brilliances of up to nine orders of magnitude higher than those of present-day synchrotron sources, will open the pathway to study, for the first time, nonlinear optical processes in the x-ray regime [6]. Multiphoton physics in the short-wavelength regime will differ considerably from the optical high-intensity regime. In contrast to the optical regime, where even single ionization typically involves many photons, the photons in the x-ray regime may carry enough energy for one-photon ionization processes. It is, however, incorrect to assume that the rate of sequential ionization events in the high-intensity x-ray regime is determined by the average peak intensity of the radiation field. One purpose of this paper is to demonstrate that these sequential processes are correlated and are governed by higher-order coherence properties of the radiation field. This implies that for interpreting experiments and for determining fundamental cross sections for nonlinear processes, statistical properties of the radiation source have to be taken into account. The second purpose of this paper is to characterize the dominant x-ray induced processes and assess their sensitivity on field coherence properties. We focus on nonlinear optical processes that may be expected to be of relevance in the initial parameter regime of LCLS (the first x-ray FEL to come online).

The x-ray FELs under construction are based on the so-called SASE (self-amplified spontaneous emission) principle [15,16]. The properties of SASE FEL radiation derive from the random arrival times of electrons in an electron bunch entering the undulator. Analytical theories, which exist only for the unsaturated gain regime, predict that SASE FEL radiation is completely chaotic [17–20] and thus characterized by irreproducible pulses. Each pulse consists of a random number of intensity spikes (coherent regions) of random amplitude. This limits the longitudinal coherence time of SASE FEL radiation in the x-ray regime near 1 keV to a few femtoseconds [21,22]. The total pulse energy fluctuates and also the spectrum varies on a shot-to-shot basis. Experiments at SASE FEL test lines show signatures of this chaotic behavior [23–28].

Basically there are two strategies for performing experiments with a SASE FEL. One possibility is a single-shot experiment. Depending on the sensitivity of the optical processes to be investigated, the pulse has to be characterized by its total energy, its spectrum, or its complete time structure. Data taken over several shots would have to be post-sorted and analyzed for each shot individually. A second strategy is to adopt a statistical approach. Then the relevant and necessary information about the radiation field can be reduced to statistical correlation functions of the electric field [29–33]. Hence a shot-to-shot characterization of the source is not needed.

The importance of field statistics in nonlinear optical processes was theoretically discovered in the early 1960s [29–40]. Experimental investigations soon thereafter studied multiphoton absorption of single-mode vs multimode laser fields [41,42], two-photon absorption of phase-diffusing [43,44] and randomly amplitude-modulated [45] laser fields, and the dependence of second-order harmonic generation on statistical properties of the incident light [46,47]. The importance of the chaoticity of SASE FEL pulses was recently theoretically examined [48] to explain the surprisingly high charge states observed in experiments on Xe gas using the Hamburg vacuum ultraviolet (vuv) FEL [49].

The paper is organized as follows. A short outline of the formalism of density matrices and quantum electrodynamics is given in Sec. II. In order to familiarize the reader with this technique and its implications, Sec. III provides a brief discussion of one-photon ionization. Section IV introduces two basic x-ray two-photon ionization processes and analyzes the dependence of double-core-hole formation on field statistics. Numerical studies on helium and neon at typical LCLS parameters are presented in Sec. V. Conclusions are drawn in Sec. VI. Atomic units ($\hbar=|e|=m=1$ and $c=1/\alpha$, where α is

the fine-structure constant) are used throughout unless otherwise stated.

II. FORMALISM

The total Hamiltonian is the sum of the atomic Hamiltonian, the electromagnetic-field Hamiltonian, and the matter-field interaction $\hat{H}^I$, which in Coulomb gauge reads

$$\hat{H}^I = \sum_{j=1}^{N_{el}} \left\{ \alpha \hat{\boldsymbol{A}}(\boldsymbol{r}_j) \cdot \hat{\boldsymbol{p}}_j + \frac{\alpha^2}{2} \hat{A}^2(\boldsymbol{r}_j) \right\}. \tag{1}$$

Here, N_{el} denotes the number of electrons, and the vector potential $\hat{\boldsymbol{A}}$ is given by

$$\hat{\boldsymbol{A}}(\boldsymbol{r}) = \frac{1}{2\pi\alpha} \sum_{\lambda} \int d^3k \omega_k^{-1/2} (\boldsymbol{\epsilon}_\lambda(\boldsymbol{k}) \hat{a}_\lambda(\boldsymbol{k}) e^{i\boldsymbol{k}\cdot\boldsymbol{r}} + \boldsymbol{\epsilon}_\lambda^*(\boldsymbol{k}) \hat{a}_\lambda^\dagger(\boldsymbol{k}) e^{-i\boldsymbol{k}\cdot\boldsymbol{r}}). \tag{2}$$

In this expression, $\hat{a}_\lambda(\boldsymbol{k})$ $[\hat{a}_\lambda^\dagger(\boldsymbol{k})]$ denotes the photon annihilation [creation] operator of mode $(\boldsymbol{k},\lambda)$ with photon energy ω_k; $\lambda=1,2$ labels the polarization. The photon annihilation and creation operators satisfy the usual commutation rules for bosonic fields. Spin contributions to $\hat{H}^I$ are neglected in this work. The use of quantum electrodynamics is not critical for the description of photoabsorption. However, it anticipates applications such as Compton scattering that are not amenable to a classical treatment of the radiation field.

The coherence properties of x-ray FEL pulses may be described utilizing a density-matrix formalism known from nonlinear statistical optics [29,32,40]. This allows one to express the probability of a specific nonlinear optical process in terms of field correlation functions. At time $t \to -\infty$, the atomic system is supposed to be in a pure state $|\Psi_i\rangle$; the FEL pulse is represented by a statistical mixture,

$$\hat{\rho}_i^R = \sum_{\{n\},\{n'\}} \rho^R_{\{n\},\{n'\}} |\{n\}\rangle\langle\{n'\}|, \tag{3}$$

where the sum goes over all possible field configurations $\{n\}=(n_{\kappa_1}, n_{\kappa_2}, \ldots)$ [n_{κ_1} denotes the number of photons in mode $\kappa_1 \equiv (\boldsymbol{k}_1, \lambda_1)$]. The state of the combined atom-field system long after the interaction of the FEL pulse with the atom is determined by the interaction-picture time-evolution operator $\hat{U}(t,t')$ via

$$\hat{\rho}_f = \lim_{t\to\infty} \lim_{t'\to-\infty} \hat{U}(t,t') [|\Psi_i\rangle\langle\Psi_i| \otimes \hat{\rho}_i^R] \hat{U}^\dagger(t,t'). \tag{4}$$

The final-state density matrix $\hat{\rho}_f$ may be calculated using perturbation theory with respect to the operators $\alpha\hat{\boldsymbol{A}}\cdot\hat{\boldsymbol{p}}$ and $\alpha^2\hat{A}^2/2$ in Eq. (1). In this paper, we concentrate on absorption processes induced by $\alpha\hat{\boldsymbol{A}}\cdot\hat{\boldsymbol{p}}$.

Ionization yields from an atomic-gas sample are insensitive to transverse coherence properties of the radiation field. The upcoming x-ray FELs will have angular beam divergences of the order of 10^{-5} radians [21]. Thus for our purposes, x-ray FEL radiation propagates in a single direction, in the following assumed to be the positive z direction. We assume that the x-ray FEL radiation is linearly polarized along the x axis and omit the polarization index λ in the following.

The average photon energy of the FEL photon bunch is denoted by ω_0. In the case of LCLS, ω_0 may be chosen in the range from 800 eV to 8 keV [3]. In light atoms, photoabsorption in this energy range promotes one or more K-shell electrons to the continuum. (The K-shell binding energy of light atoms such as carbon or oxygen is smaller by a few hundred eV than the lowest photon energy available at LCLS.) We will assume that ω_0 is sufficiently high so that near-threshold effects may be neglected. LCLS will have a relative bandwidth of the order of 10^{-4} [22]. A consequence of this is that the electronic transition matrix elements are constant over the relatively narrow spectral bandwidth of the FEL. This is exploited throughout.

III. ONE-PHOTON IONIZATION

Consider an N-electron atom, initially in its ground state $|\Psi_0^N\rangle$, that becomes singly ionized via one-photon absorption. Let $\boldsymbol{q}$ denote the momentum of the photoelectron emitted into the infinitesimal solid-angle element $d\Omega_q$. We assume for simplicity that the spectral bandwidth of the FEL pulses is small enough so that measurement of the photoelectron energy $E_q=q^2/2$ allows one to identify the state $|\Psi_r^{N-1}\rangle$ of the residual ion. (There may be degeneracies, but this is irrelevant here.) Let I_r^{N-1} denote the ionization potential associated with the production of $|\Psi_r^{N-1}\rangle$. We symbolize the final state of the N-electron system by $|\boldsymbol{q},\Psi_r^{N-1}\rangle$, which may be taken to be energy-normalized [50]. The differential probability of exciting the atom to the state $|\boldsymbol{q},\Psi_r^{N-1}\rangle$ is the expectation value of the observable $|\boldsymbol{q},\Psi_r^{N-1}\rangle\langle\boldsymbol{q},\Psi_r^{N-1}|$ with respect to the density matrix $\hat{\rho}_f$ [Eq. (4)], i.e.,

$$\frac{d^2P(\boldsymbol{q},\Psi_r^{N-1})}{dE_q d\Omega_q} = \mathrm{Tr}\{|\boldsymbol{q},\Psi_r^{N-1}\rangle\langle\boldsymbol{q},\Psi_r^{N-1}|\hat{\rho}_f\}. \tag{5}$$

The trace in this expression is performed over the unobserved degrees of freedom of the radiation field.

One-photon absorption is a first-order process with respect to $\alpha\hat{\boldsymbol{A}}\cdot\hat{\boldsymbol{p}}$ [Eq. (1)]. From Eq. (5) it follows, upon integration over the narrow photoelectron spectral profile centered at $q_0^2/2=\omega_0-I_r^{N-1}$, that

$$\frac{dP(\boldsymbol{q}_0,\Psi_r^{N-1})}{d\Omega_q} = \frac{d\sigma_0^{(1)}}{d\Omega_q}(\omega_0,\boldsymbol{q}_0)\mathcal{J}^{(1)}. \tag{6}$$

Here,

$$\frac{d\sigma_0^{(1)}}{d\Omega_q} = \alpha\frac{(2\pi)^2}{\omega_0} |\langle\boldsymbol{q}_0,\Psi_r^{N-1}|\sum_j e^{i\alpha\omega_0 z_j} \hat{\boldsymbol{p}}_j\cdot\boldsymbol{\epsilon}_x|\Psi_0^N\rangle|^2 \tag{7}$$

is the differential cross section for one-photon ionization, $\boldsymbol{\epsilon}_x$ is the polarization vector (unit vector along the x axis),

$$\mathcal{J}^{(1)} = \int_0^\infty d\omega \frac{G^{(1)}(\omega,\omega)}{(2\pi)^2} \tag{8}$$

is the average number of photons per unit area and FEL pulse, and

$$G^{(1)}(\omega,\omega') = \alpha\,\mathrm{Tr}[\hat{a}^{\dagger}(\alpha\omega)\hat{a}(\alpha\omega')\hat{\rho}_i^R] \tag{9}$$

is the field correlation function of first order. Photoionization experiments at existing synchrotron radiation facilities are characterized by one-photon absorption. The high peak intensity of future x-ray FELs will make it possible to induce two-photon and higher-order processes.

IV. TWO-PHOTON IONIZATION

To second order with respect to $\alpha\hat{\boldsymbol{A}}\cdot\hat{\boldsymbol{p}}$, the (differential) probability, per FEL pulse, for a two-photon transition from an initial atomic state $|\Psi_i\rangle$ (energy E_i) to a final atomic state $|\Psi_f\rangle$ (energy E_f, width Γ_f) is given by

$$\begin{aligned} P(\omega_{fi}) = {} & \frac{\alpha^2}{(2\pi)^2}\int_0^\infty d\tilde{\omega}\frac{1}{\pi}\frac{\Gamma_f/2}{(\omega_{fi}-\tilde{\omega})^2+\Gamma_f^2/4} \\ & \times \int_0^\infty d\omega \int_0^\infty d\omega' \frac{G^{(2)}(\tilde{\omega}-\omega,\omega,\omega',\tilde{\omega}-\omega')}{\sqrt{\omega(\tilde{\omega}-\omega)\omega'(\tilde{\omega}-\omega')}} \\ & \times m_{fi}(\omega,\tilde{\omega}-\omega)^* m_{fi}(\omega',\tilde{\omega}-\omega'). \end{aligned} \tag{10}$$

Here, $\omega_{fi}=E_f-E_i$, and

$$\begin{aligned} m_{fi}(\omega,\omega') = {} & \sum_l \langle\Psi_f|\sum_j e^{i\alpha\omega z_j}\hat{\boldsymbol{p}}_j\cdot\boldsymbol{\epsilon}_x|\Psi_l\rangle \\ & \times \frac{\langle\Psi_l|\sum_j e^{i\alpha\omega' z_j}\hat{\boldsymbol{p}}_j\cdot\boldsymbol{\epsilon}_x|\Psi_i\rangle}{\omega_{li}-\omega'-i\Gamma_l/2}. \end{aligned} \tag{11}$$

The two-photon absorption probability, Eq. (10), is governed by the second-order correlation function

$$G^{(2)}(\omega_1,\omega_2,\omega_3,\omega_4) = \alpha^2\mathrm{Tr}[\hat{a}^{\dagger}(k_1)\hat{a}^{\dagger}(k_2)\hat{a}(k_3)\hat{a}(k_4)\hat{\rho}_i^R], \tag{12}$$

where $k_i=\alpha\omega_i$. Certain second-order coherence properties of radiation fields may be measured using intensity interferometry methods [51–54].

At high photon energy, the atomic response is dominated by inner-shell electrons. The $\alpha\hat{\boldsymbol{A}}\cdot\hat{\boldsymbol{p}}$ interaction to second order acts effectively as a two-body operator. Hence, even when electron-correlation effects are neglected, the two-photon amplitude $m_{fi}(\omega,\omega')$ in Eq. (11) may describe the excitation of two inner-shell electrons. (Note that in 1% or less of all *one-photon* absorption events, electron-electron interaction induces the emission of two K-shell electrons [55].) Qualitatively, we may therefore distinguish the following two x-ray two-photon processes: (i) The first photon ionizes a K-shell electron; Auger decay takes place, thereby filling the K-shell hole; and the second photon ionizes another K-shell electron. We refer to this process as PAP. (ii) After ionization of a first K-shell electron, the second K-shell electron is ionized before Auger decay takes place. We call this process PPA. Both processes, which are followed by various relaxation processes, are described by Eq. (10). Particularly, they are determined by the second-order correlation function of the photon field.

The PPA process, which leads to double-core-hole formation, is a sensitive probe of the time evolution of the x-ray intensity during a FEL pulse. It may only be observed with high probability if photoabsorption occurs within an Auger lifetime, i.e., within a few fs. Otherwise, the PAP process will be more relevant. PPA is the case we will focus on in this section; PAP can be treated in a similar fashion by taking electron-electron interaction into account in the intermediate states $|\Psi_l\rangle$ in Eq. (11).

Following the absorption of the first photon, the residual ion is (temporarily) in the core-excited state $|\Psi_r^{N-1}\rangle$. The second photon may produce the double-K-hole state $|\Psi_s^{N-2}\rangle$. Generally, the energy I_s^{N-2} needed to remove the second K-shell electron in the state $|\Psi_r^{N-1}\rangle$ is greater than the energy I_r^{N-1} required for the first K-shell electron. Let $\Delta I=I_s^{N-2}-I_r^{N-1}$. Hartree-Fock-Slater calculations we have performed give $\Delta I(\mathrm{Be})=44$ eV, $\Delta I(\mathrm{C})=60$ eV, $\Delta I(\mathrm{O})=77$ eV, and $\Delta I(\mathrm{Ne})=94$ eV. (These results are accurate to within about 30%.) Since the two final-state photoelectrons are fast, their mutual repulsion may be neglected. In practice, this means that the energy $q_1^2/2=\omega_0-I_r^{N-1}$ of the electron first ionized is unaffected by the second ionization event, which produces a photoelectron with energy $q_2^2/2=\omega_0-I_s^{N-2}$. Consequently, within the spectral bandwidth of an x-ray FEL, the two photoelectrons are distinguishable.

Using a straightforward generalization of the sudden approximation [56], it thus follows from Eq. (10), after integration over the respective photoelectron line profiles, that the doubly differential two-photon double-ionization probability per FEL pulse is

$$\frac{d^2P}{d\Omega_{q_1}d\Omega_{q_2}} = \frac{d\sigma_0^{(1)}}{d\Omega_{q_1}}(\omega_0,\boldsymbol{q}_1)\frac{d\sigma_r^{(1)}}{d\Omega_{q_2}}(\omega_0,\boldsymbol{q}_2)\mathcal{J}_r^{(2)}. \tag{13}$$

The differential cross section $d\sigma_0^{(1)}/d\Omega_{q_1}$ for one-photon ionization of the ground-state atom is defined in Eq. (7). The differential cross section for one-photon ionization of the core-excited ion is

$$\frac{d\sigma_r^{(1)}}{d\Omega_{q_2}} = \alpha\frac{(2\pi)^2}{\omega_0}|\langle\boldsymbol{q}_2,\Psi_s^{N-2}|\sum_j e^{i\alpha\omega_0 z_j}\hat{\boldsymbol{p}}_j\cdot\boldsymbol{\epsilon}_x|\Psi_r^{N-1}\rangle|^2. \tag{14}$$

The quantity

$$\begin{aligned} \mathcal{J}_r^{(2)} = {} & \frac{1}{(2\pi)^5}\int_0^\infty d\tilde{\omega}\int_0^\infty d\omega\int_0^\infty d\omega' \\ & \times \frac{G^{(2)}(\tilde{\omega}-\omega,\omega,\omega',\tilde{\omega}-\omega')}{\Gamma_r^{N-1}-i(\omega-\omega')} \end{aligned} \tag{15}$$

appearing in Eq. (13) depends on the decay rate Γ_r^{N-1} of the intermediate state $|\Psi_r^{N-1}\rangle$ in such a way that if Γ_r^{N-1} is very large, then double-K-hole formation is suppressed.

Using the quantum-mechanical definition of the Poynting vector $\hat{S}$ [57], the photon flux operator may be approximated by $\hat{j}=\hat{S}/\omega_0$. In the limit of very high photon number, which is applicable in the case of an x-ray FEL, it may thus be shown that

$$\mathcal{J}_r^{(2)} = \left\langle \int_{-\infty}^{\infty} dt \hat{j}(t) \int_{-\infty}^{t} dt' \hat{j}(t') e^{-\Gamma_r^{N-1}(t-t')} \right\rangle, \tag{16}$$

where $\langle \cdots \rangle$ signals that an average over an ensemble of FEL pulses is taken. Note that $\mathcal{J}_r^{(2)}$ is generally different from

$$\tilde{\mathcal{J}}_r^{(2)} = \int_{-\infty}^{\infty} dt \langle \hat{j}(t) \rangle \int_{-\infty}^{t} dt' \langle \hat{j}(t') \rangle e^{-\Gamma_r^{N-1}(t-t')}. \tag{17}$$

A SASE FEL pulse consists of subpulses. The number of these subpulses and the subpulse durations, amplitudes, and phases fluctuate from shot to shot in a random manner [24–26]. For such a chaotic radiation field, the second-order correlation function satisfies the Siegert relation [18,30,58]. Treating the radiation field as a classical variable, it follows that

$$\mathcal{J}_r^{(2)} = \int_{-\infty}^{\infty} dt \langle \hat{j}(t) \rangle \int_{-\infty}^{t} dt' \langle \hat{j}(t') \rangle \times e^{-\Gamma_r^{N-1}(t-t')} \{1 + |g^{(1)}(t,t')|^2\}. \tag{18}$$

The normalized first-order correlation function $g^{(1)}(t,t')$ (cf. Ref. [29]) is equal to unity if $t-t' \geq 0$ is much smaller than the coherence time τ, and $g^{(1)}(t,t')$ vanishes if $t-t' \gg \tau$. The exponential factor appearing in Eqs. (16)–(18) restricts $t-t'$ to values smaller than $\sim 1/\Gamma_r^{N-1}$. Hence the relative importance of the difference between $\mathcal{J}_r^{(2)}$ and $\tilde{\mathcal{J}}_r^{(2)}$ depends on $\xi_r = \Gamma_r^{N-1}\tau$. If $\xi_r \gg 1$, then $\eta = \mathcal{J}_r^{(2)}/\tilde{\mathcal{J}}_r^{(2)} \approx 2$; if $\xi_r \ll 1$, then $\eta \approx 1$, assuming that τ is small in comparison to the average FEL pulse duration. The coherence time of LCLS operating in the soft x-ray regime is expected to be several femtoseconds [22], so that for core-excited $|\Psi_r^{N-1}\rangle$, ξ_r is of the order of 1. The consequences of this are explored numerically in Sec. V, where both PPA and PAP processes are discussed further.

Assuming that the radiation field is in a single-mode coherent state, Eqs. (13) and (16) allow us to determine the two-photon double ionization cross section:

$$\frac{d^2\sigma_0^{(2)}}{d\Omega_{q_1} d\Omega_{q_2}} = \frac{d\sigma_0^{(1)}}{d\Omega_{q_1}} \frac{d\sigma_r^{(1)}}{d\Omega_{q_2}} \frac{1}{\Gamma_r^{N-1}}. \tag{19}$$

In Sec. V, we analyze x-ray multiphoton ionization of neon. Utilizing Eq. (19), the cross section for double-K-hole formation in Ne via two-photon absorption can be estimated. The double-K-hole threshold of Ne lies at $2\omega_0 = 1863$ eV [55]. Thus since the K-shell single-ionization potential of Ne is 870 eV [59], it takes at least $\omega_0 = 993$ eV to ionize the second K-shell electron in core-ionized Ne. Since the one-photon core ionization cross section of Ne near $\omega_0 = 1$ keV is of the order of 100 kb and the Auger lifetime of core-ionized Ne is 2.4 fs [59], we estimate a double-K-hole cross section of the order of 10^{-53} cm^4 s. As far as we know, Ref. [60] performs the only other theoretical analysis of two-photon double-K-hole formation (also in Ne). The double-K-hole cross section calculated in Ref. [60] displays a monotonic behavior above $\omega_0 = 993$ eV, as we would expect. Surprisingly, their calculated cross section near $\omega_0 = 1$ keV is of the order of 10^{-49} cm^4 s. As pointed out earlier, we focus here on high photon energies and disregard near-threshold effects. Only in this limit may Eq. (19) be expected to be valid. However, it seems unlikely in our opinion that Eq. (19) should underestimate the double-K-hole cross section by four orders of magnitude. Future *ab initio* studies should help resolve this issue.

V. NUMERICAL STUDIES

A. Approach

In order to investigate the response of atoms to intense x-ray radiation and to demonstrate the impact of chaotic photon statistics, we numerically solve a set of coupled rate equations for an ensemble of radiation pulses. It is easy to see that this approach captures the essential physics. Consider an N-electron atom initially in its ground state, i.e., before the FEL pulse the occupation probability of this state is $P_0^N = 1$. Photoionization (cross section $\sigma_0^{(1)}$) converts the atom to an ion in the state $|\Psi_r^{N-1}\rangle$ (occupation probability P_r^{N-1}), which in turn may be either photoionized (cross section $\sigma_r^{(1)}$) or undergo Auger decay (decay rate Γ_r^{N-1}). If photoionization takes place, the ion is excited to the $(N-2)$-electron state $|\Psi_s^{N-2}\rangle$, which may decay at a rate of Γ_s^{N-2}:

$$\dot{P}_0^N(t) = -\sigma_0^{(1)} j(t) P_0^N(t), \tag{20}$$

$$\dot{P}_r^{N-1}(t) = \sigma_0^{(1)} j(t) P_0^N(t) - \sigma_r^{(1)} j(t) P_r^{N-1}(t) - \Gamma_r^{N-1} P_r^{N-1}(t), \tag{21}$$

$$\dot{P}_s^{N-2}(t) = \sigma_r^{(1)} j(t) P_r^{N-1}(t) - \Gamma_s^{N-2} P_s^{N-2}(t). \tag{22}$$

These equations are sufficient to describe PPA from the ground state (see Sec. IV). The PPA two-photon absorption probability is given by

$$P_{\mathrm{PPA}} = \sigma_r^{(1)} \int_{-\infty}^{\infty} dt j(t) P_r^{N-1}(t). \tag{23}$$

Using Eqs. (20) and (21), P_r^{N-1} may be determined to leading order in $j(t)$ and may be inserted into Eq. (23). After averaging over an ensemble of FEL pulses, P_{PPA} is found to be consistent with the quantum-mechanical result, Eqs. (13) and (16).

Let the ion following Auger decay of $|\Psi_r^{N-1}\rangle$ be in the $(N-2)$-electron state $|\Psi_t^{N-2}\rangle$ (generally, there are of course several Auger channels). This state, in which both vacancies are in the valence shell, may be further photoionized (cross section $\sigma_t^{(1)}$). Hence

$$\dot{P}_t^{N-2}(t) = \Gamma_r^{N-1} P_r^{N-1}(t) - \sigma_t^{(1)} j(t) P_t^{N-2}(t). \tag{24}$$

From this we obtain the PAP two-photon absorption probability (Sec. IV) to leading order in $j(t)$:

$$P_{\mathrm{PAP}} = \sigma_0^{(1)} \Gamma_r^{N-1} \sigma_t^{(1)} \int_{-\infty}^{\infty} dt j(t) \times \int_{-\infty}^{t} dt' \int_{-\infty}^{t'} dt'' j(t'') e^{-\Gamma_r^{N-1}(t'-t'')}. \quad (25)$$

When this expression is averaged over an ensemble of chaotic radiation pulses, P_{PAP} may be written, in analogy to Eq. (18), in terms of $\langle j(t)\rangle\langle j(t'')\rangle\{1+|g^{(1)}(t,t'')|^2\}$. However, the Auger rate Γ_r^{N-1} in Eq. (25) restricts $t'-t''$, not $t-t''$. Therefore in contrast to the PPA process (Sec. IV), no matter whether the Auger lifetime is long or short in comparison to the coherence time, the ensemble-averaged PAP two-photon absorption probability does not display any significant statistical enhancement, again assuming that the coherence time is much shorter than the pulse duration.

In order to efficiently simulate an ensemble of chaotic radiation pulses we adopt an approach developed in Ref. [61]. Within this model, the electric field amplitude of each mode is a Gaussian random variable with zero mean and a variance equal to the power spectrum at the associated frequency. We choose a Gaussian power spectrum centered at frequency ω_0 with a variance corresponding to the relative LCLS gain bandwidth of 4.4×10^{-4} [22]. The intensity as a function of time is determined by applying the fast Fourier transform algorithm to the representation of the electric field in frequency space. We employ a masking function in the time domain to smoothly turn the pulses on and off. The ensemble average is a square pulse with rise and fall times equal to 1% of the total pulse duration T. The sampling width in ω space is $2\pi/T$. The number of independent modes determines the temporal resolution. We choose $T=230$ fs [21] and include 12 288 independent modes. The total energy per pulse is distributed according to a Gamma distribution, in agreement with analytic predictions for SASE FEL radiation in the unsaturated gain regime [20]. The relative width of the pulse energy distribution is given by $\sqrt{\tau/T}$ [20] (τ is the coherence time) and equals about 10% for the parameters employed. The average number of photons per pulse assumed is 1×10^{13} [21]. The coupled rate equations are solved, utilizing a fourth-order Runge-Kutta integrator, for both an ensemble of 10 000 pulses and the ensemble-averaged pulse. Before each pulse, the atom considered is assumed to be in its neutral ground state. Our numerical calculations are based on a transverse pulse profile that is circular with a uniform intensity distribution inside the circle. Spatial averaging, which would be necessary for nonuniform intensity distributions, is not performed.

B. Helium

The simplest system for which two-photon double ionization exists is helium. In view of the relatively small x-ray interaction cross section of low-Z elements, it is critical to determine whether the photon flux of the upcoming x-ray FEL facilities is high enough for a statistically significant count rate. Figure 1(a) shows the helium charge-state probability after the end of a FEL pulse, at a photon energy of 870 eV, as a function of the focal diameter. We may conclude from Fig. 1(a) that the two-photon double ionization probability per atom is a percent or so at a focal diameter of 2 μm, reaching 100% near 0.25 μm.

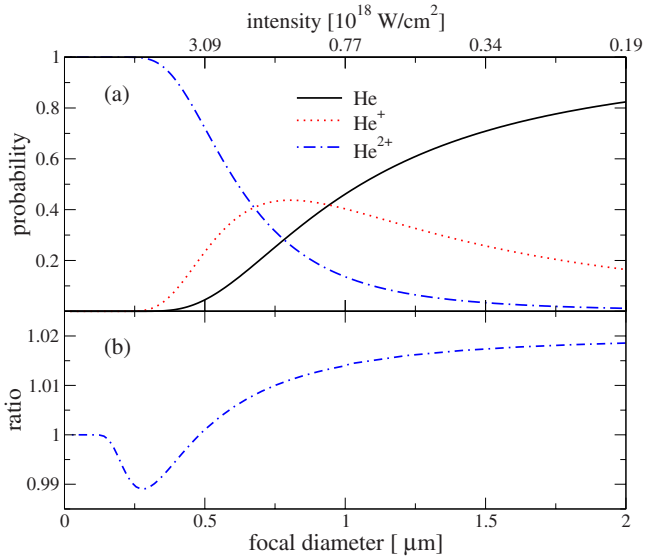

FIG. 1. (Color online) (a) Probability, as a function of the focal diameter, of observing He, He^+, or He^{2+}, after exposure of neutral helium to an 870-eV FEL pulse. (b) The ensemble average of the He^{2+} yield divided by the He^{2+} yield obtained with the ensemble-averaged radiation pulse.

The data underlying Fig. 1(a) were obtained by numerical solution of Eqs. (20)–(22). Evidently, in the case of helium, $\Gamma_r^{N-1}=\Gamma_s^{N-2}=0$. The photoabsorption cross sections were calculated using the Los Alamos National Laboratory Atomic Physics Codes [62]. At $\omega_0=870$ eV, we find $\sigma_0^{(1)}=610$ b and $\sigma_r^{(1)}=420$ b. (The experimentally determined photoionization cross section of He at 850 eV is 572 b, with an estimated uncertainty of ±10% [63].) In the photon energy range below 3 keV, ionization by Compton scattering may be neglected [64–66]. Also neglected in our simple model are electron-correlation-induced excitation processes. For instance, following one-photon absorption of He, the production of He^+ in its ground state is about 17 times more likely than the production of He^+ in any bound excited state [67]. The ratio of cross sections of correlation-induced double ionization versus single ionization of helium at a photon energy of 870 keV is 2.6% [68,69]. Figure 1(a) demonstrates that for focal diameters smaller than 2 μm, the probability of two-photon double ionization exceeds that of the correlation-induced process. (The latter has an absolute probability of no more than 0.01.) By measuring the energy of the two photoelectrons, both double-ionization processes can be distinguished.

The probabilities shown in Fig. 1(a) are insensitive to the temporal pulse shape chosen. The ensemble-averaged pulse mentioned earlier and a Gaussian pulse profile give virtually indistinguishable results. The effect of chaoticity of the radiation field is small, as evidenced by Fig. 1(b), where we show the ratio η of the ensemble-averaged He^{2+} yield and the He^{2+} yield from the ensemble-averaged pulse. For large focal diameters, i.e., as the perturbative limit is approached,

η is greater than 1 by almost 2%. This is easily understood by reference to Eq. (18): Since He^+ in its ground state cannot decay, the second photon can be absorbed at any time during the pulse duration T (after absorption of the first photon). Statistical enhancement of two-photon absorption, however, occurs over a time interval corresponding to the coherence time τ. The fraction τ/T is of the order of 1% in our calculations. This limits the statistical enhancement that may be observed. At very small focus, He^{2+} production is saturated and η must equal 1. It is interesting to observe that η does not approach the high-intensity limit in a monotonic fashion; a pronounced minimum appears in Fig. 1(b) near a focal diameter of 0.3 μm. In this regime, helium ionization is saturated [see Fig. 1(a)], and the perturbative arguments used in Sec. IV are not applicable.

C. Neon

Some of the first experiments with LCLS will involve neon [7]. The ionization cross sections for neon and its ions are considerably larger in the x-ray regime than for helium, and more complex processes can be studied. Particularly, if the photon energy is high enough, photoabsorption leads to the formation of an inner-shell vacancy, which is electronically metastable. In contrast to He, a 1s hole in Ne has a lifetime (2.4 fs) comparable to the coherence time of LCLS (2.6 fs at a photon energy of 1050 eV [22]). The core hole either decays followed by the absorption of an x-ray photon (PAP process), or, if the intensity of the field is high enough, another photon is absorbed, thereby producing a double-core hole, which relaxes via Auger decay (PPA process) and gives rise to the hypersatellite structure in the Auger electron spectrum [55]. According to Eqs. (13) and (18), field statistics may be expected to enhance the PPA process.

In order to assess for Ne the impact of SASE-FEL chaoticity and the relative importance of the PAP and PPA processes, we solved a set of rate equations similar to Eqs. (20)–(22) and (24). Ionization cross sections were calculated [62] for valence and core shells of Ne^{q+} in various electronic configurations ($q=0,1,\ldots$). Auger decay of core holes and double-core holes was taken into account by using Auger decay rates from Ref. [70]. For Ne^{8+} and Ne^{9+} we also included decay by fluorescence [70]. In total, 158 different channels were treated. Not included in our model are shake-off processes [71] and double-Auger decay [72].

By keeping track of the Auger yield from single- or double-core hole configurations, it may be monitored whether a given two-photon absorption event is a PAP or PPA process. (In the case of the double-core hole, Auger yield refers to the first Auger decay step in the decay cascade.) Figure 2 shows the time evolution of the system over the first few fs of a typical FEL sample pulse with a photon energy of $\omega_0=1050$ eV (chosen to lie above the K-shell ionization threshold of Ne^{1+} $1s^12s^22p^6$). Within the first 10 fs, Ne^{1+} and Ne^{2+} production is saturated. In Fig. 2(a), the Auger decay rate of Ne^{1+} $1s^12s^22p^6$ is compared with the K-shell photoionization rate of Ne^{1+} $1s^12s^22p^6$ (ionization cross section times photon flux). A few fs after the beginning of the pulse, the K-shell photoionization rate exceeds the

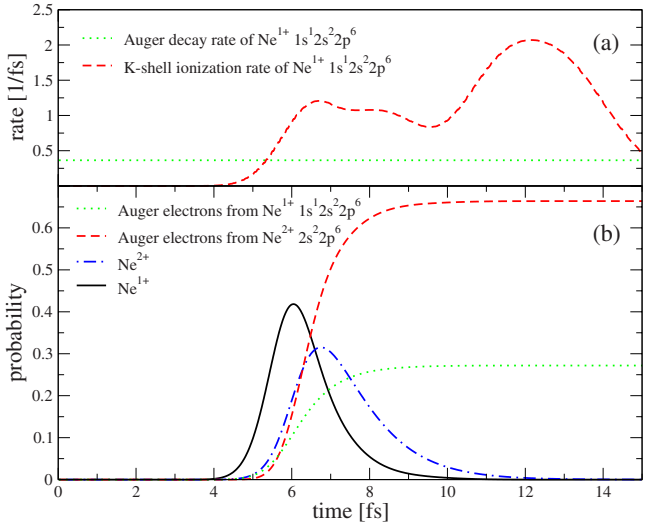

FIG. 2. (Color online) Neon exposed to a typical FEL pulse with $\omega_0=1050$ eV and a focal diameter of 1 μm. The first few fs during the pulse are shown. (a) K-shell photoionization rate of Ne^{1+} $1s^12s^22p^6$, as a function of time. Also plotted is the Auger decay rate of a Ne core hole. (b) Ne^{1+} and Ne^{2+} probabilities and Auger yields from Ne^{1+} $1s^12s^22p^6$ and Ne^{2+} $2s^22p^6$, as a function of time.

Auger decay rate. As may be seen in Fig. 2(b), this coincides with the time interval during which the production of Ne^{1+} $1s^12s^22p^6$ and the subsequent transition to Ne^{2+} are efficient. Therefore for the sample pulse considered, PPA dominates over PAP, as signaled by the Auger yields shown in Fig. 2(b): The Auger hypersatellite yield from the double-core hole (Ne^{2+} $2s^22p^6$) is more than two times as large as the Auger yield from Ne^{1+} $1s^12s^22p^6$.

Figure 3(a) shows the ensemble-averaged Auger electron yields originating from the single-core-hole states of Ne^{1+} and Ne^{3+} compared to the yields resulting from the double-core-hole states of Ne^{2+} and Ne^{4+} as a function of the focal diameter. At focal diameters of several μm or larger, the PAP process dominates and the ionization of neon proceeds in a sequence of inner-shell photoionization and Auger-decay events. (The main channel for producing Ne^{6+} follows the pattern PAPAPA.) At approximately 1.5 μm, PAP and PPA processes are of equal importance, whereas at focal diameters below 1 μm, PPA clearly dominates. The mechanisms that lead to the production of the double-core-hole state of Ne^{4+} may be written as PAPP and PPAP. At a focal diameter of 1 μm, both mechanisms contribute with approximately equal probability. In Fig. 3(b), we plot the ratio η of the ensemble average of the Auger electron yield in a given channel and the corresponding Auger electron yield obtained with the averaged pulse. At large focal widths (approximately 100 μm), η for the Ne^{2+} double-core hole tends to 1.36, whereas η for the Ne^{4+} double-core hole tends to 1.31. These statistical enhancement factors are roughly halfway between the two extremes of $\eta=1$ and $\eta=2$ discussed in Sec. IV. This is consistent with the fact that here the ratio of the coherence time and the respective Auger lifetime of the intermediate single-core-hole state is approximately equal to 1.

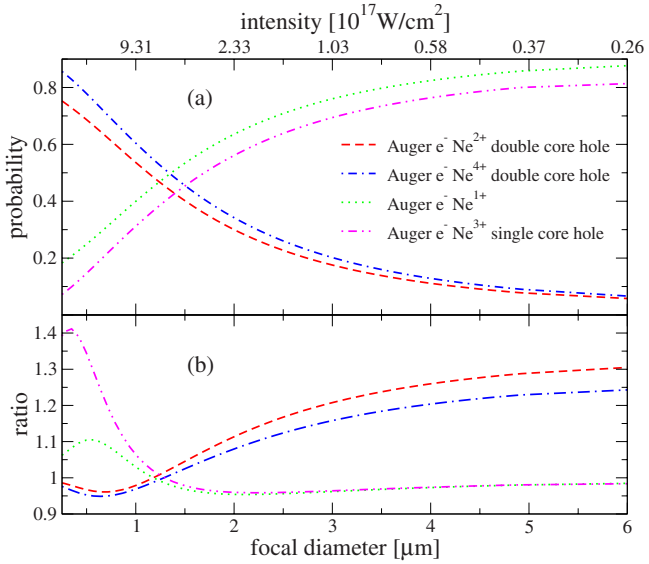

FIG. 3. (Color online) Neon exposed to an ensemble of 10 000 FEL pulses (ω_0=1050 eV). (a) Auger electron yields (ensemble average) from the double-core-hole states of Ne^{2+} and Ne^{4+} (PPA process) and from the single-core-hole states of Ne^{1+} and Ne^{3+} (PAP process), as a function of the focal diameter. (b) Ratio of the ensemble average of Auger electron yield and the corresponding yield obtained with the averaged pulse.

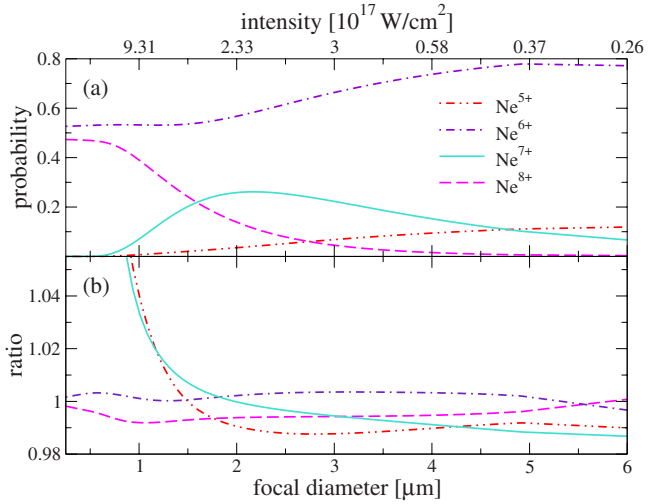

FIG. 4. (Color online) Neon exposed to an ensemble of 10 000 FEL pulses (ω_0=1050 eV). (a) Probability to observe neon in a specific charge state (ensemble average), as a function of the focal diameter. (b) Ratio of the ensemble average of charge-state probability and the corresponding probability obtained with the averaged pulse.

In fact, the lifetimes of the single-core-hole states of Ne^{3+} are bigger by 12–25 % (depending on the electronic configuration of Ne^{3+}) than the lifetime of Ne^{1+} $1s^1 2s^2 2p^6$, which is the reason why η for Ne^{4+} is smaller than η for Ne^{2+}. As the Auger electron yields of Ne^{2+} and Ne^{4+} start to saturate at high intensity, the respective η's tend to unity, after passing through a minimum similar to the one observed in He (see Fig. 1). We note that at low intensity, the impact of the chaotic field statistics is to slightly suppress the η's for the Auger electron yields from the single-core-hole states of Ne^{1+} and Ne^{3+} (PAP). Both single-core-hole η's go through a pronounced maximum near a focal diameter of 0.5 μm.

At the intensities shown in Fig. 3, the charge states discussed appear and disappear relatively early during the FEL pulse (cf. Fig. 2). Their temporary presence is most easily monitored by measurement of the Auger electron spectrum. As illustrated in Fig. 4(a), the charge-state distribution after the FEL pulse is characterized by Ne ions with charge 5+ or higher. The photon energy of 1050 eV allows for K-shell ionization of up to Ne^{4+} (production of Ne^{5+} with a single core hole), which via Auger decay gives Ne^{6+}. This ion is therefore predominant in the charge-state distribution. Further ionization proceeds via valence shell ionization (symbol V), which at small focus creates up to Ne^{8+}. At a focus of approximately 1.5 μm, when PPA and PAP are of equal importance, the major routes to producing Ne^{8+} occur with similar probabilities and follow the patterns PAPAPAVV, PPAAPAVV, and PAPPAAVV. These are all five-photon processes. Hence far below saturation, the Ne^{8+} yield should be proportional to the fifth power of the intensity. We observe this expected power-law dependence at intensities smaller than 3×10^{14} W/cm^2 (corresponding to a focal diameter of 50 μm), where the probability of producing Ne^{8+} is 10^{-9}. The power-law dependence is valid only in the perturbative limit, in which the Ne ground state is hardly depopulated. This condition is clearly not satisfied in the parameter range underlying Fig. 4. In Fig. 4(b), we plot the ratio η of the ensemble-averaged charge-state probability and the corresponding probability resulting from the averaged pulse. Unlike the Auger electron yields, the ion yields are only weakly affected by the statistical properties of the radiation field; η is very close to unity. We confirmed that this is also true for higher photon energies. (An exception is discussed below.) The photon-energy dependence of the ion yield may therefore be calculated using the averaged pulse.

Figure 5 shows the Ne ion yield as a function of the photon energy (for the averaged pulse). The graph displays a complex, steplike structure. Generally, a large increase or decrease in a specific charge state is due to the opening of a new ionization channel. The K edge of Ne is located at 870 eV. For energies below 870 eV, production of Ne^{6+} involves valence-shell ionization (VVVVVV six-photon process). At the Ne K edge, there is a discontinuous increase in the Ne^{6+} (PAVVVV five-photon process) and Ne^{8+} (PAVVVVVV seven-photon process) yields. The step in the Ne^{8+} yield near 925 eV coincides with the K edge of Ne^{2+} (PAPAVVVV six-photon process). Ne^{8+} is predominant between 1100 and 1200 eV, i.e., between the K edges of Ne^{6+} and Ne^{8+}. The major pathway to Ne^{10+}, which becomes relevant above 1225 eV, involves the temporary formation of double-core-excited Ne^{8+} from core-excited Ne^{7+} (PAPAPAPP, PPAAPAPP, or PAPPAAPP). Doubly excited Ne^{8+} undergoes autoionization primarily into the n=2 channel of Ne^{9+} [73]. Fully stripped neon is then produced through photoionization of the remaining electron. Overall, this is a six-photon process. The production of Ne^{10+} rises to its maximum right above the threshold for ionizing Ne^{9+} in its ground state (1362 eV).

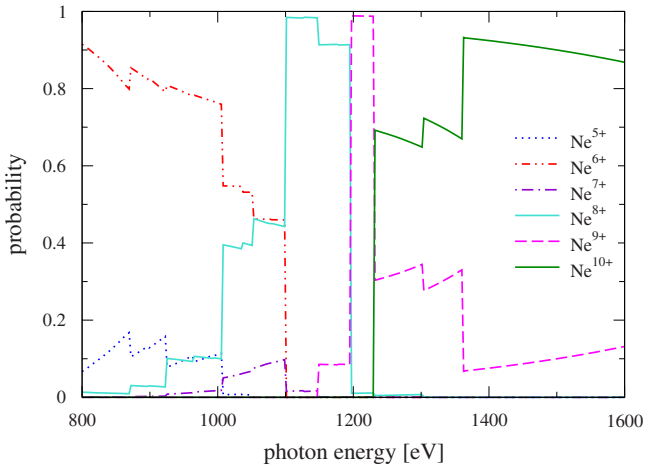

FIG. 5. (Color online) Probability of observing neon in a specific charge state after exposure to the averaged FEL pulse, as a function of the photon energy. The focal diameter was chosen as 1 μm.

The charge-state distribution of Ne is largely independent of the pulse shape if, at the photon energy considered, temporary double-core-hole formation is not essential for producing the respective charge states. For instance, when we replace the averaged pulse underlying Fig. 5 with a Gaussian pulse (same duration and pulse energy), the charge-state distribution varies by less than 5% for the dominant ion species up to Ne^{8+}. In the energy window between 1225 and 1362 eV, where the generation of doubly-core-excited Ne^{8+} is crucial in order to produce Ne^{10+}, the Ne^{10+} yield is 1.6 times bigger for the averaged pulse than for the Gaussian pulse. We mention that for the Auger electron yield originating from the double-core-hole state of Ne^{2+}, the enhancement factor for the averaged pulse relative to the Gaussian pulse is 15.

VI. CONCLUSIONS

At sufficiently high photon energy, nonlinear x-ray absorption may in general be characterized by a sequence of inner-shell photoemission and Auger decay processes. As discussed in Sec. IV, we may distinguish between two-photon processes that are accompanied by double-core-hole formation (PPA) and those associated with the formation of a core hole followed immediately by Auger decay (PAP). The PPA process is rather sensitive to the chaoticity of SASE FEL radiation; it may be enhanced by a factor of up to 2. What matters here is the ratio of the FEL coherence time and the Auger lifetime: The larger this ratio, the closer to the maximum value the enhancement factor will be. In the case of neon double-core-hole formation, assuming LCLS parameters, we find an enhancement factor of about 1.3, provided PPA is not saturated. On the other hand, in the case of the PAP process, it makes very little difference whether the PAP probability is averaged over the ensemble of radiation pulses or whether the PAP probability is determined only for the averaged radiation pulse.

Initially, LCLS will operate in the soft-x-ray regime near 1 keV. This makes both He and Ne good candidates for first experiments. Our calculations demonstrate that near a focal diameter of 1 μm, two-photon double ionization of He approaches saturation. For He, SASE FEL statistics is essentially irrelevant, since the intermediate state does not undergo relaxation and the coherence time is small in comparison to the pulse duration. In the case of Ne, we find that PPA- and PAP-type processes are of similar importance. Above 1.4 keV, Ne may become essentially fully stripped. This corresponds to a sequential six-photon process. The nonlinear nature of Ne^{10+} production, for instance, may be experimentally verified by measuring the Ne^{10+} yield as a function of the intensity. At a focal diameter of 1 μm, the Ne^{10+} yield is saturated (see Fig. 5). By attenuating the LCLS beam, or by increasing the focal width, one may reach an unsaturated regime in which the Ne^{10+} yield is proportional to the average peak pulse intensity to the power of 6.

In stark contrast to experiments with chaotic lasers in the optical domain [41,42], the statistical enhancement factor in sequential x-ray n-photon absorption is much smaller than $n!$, except for $n=2$ in the case of pure PPA. The statistical enhancement of nonlinear x-ray absorption is limited by the enhancement obtained in individual PPA steps. At low intensity, where PPA is weak, the primary mechanism for producing a given charge state is PAP. At high, nonperturbative intensity, PPA becomes important, but due to saturation effects, the statistical enhancement factor of PPA is now close to one (cf. Fig. 3). Therefore charge-state distributions may be calculated, to a first approximation, using simply the averaged radiation pulse. More sensitive probes of FEL photon statistics are the Auger electron spectra associated with the electronic decay of double-core-hole states.

ACKNOWLEDGMENTS

We thank Elliot Kanter, Bertold Krässig, Stephen Southworth, and Linda Young for helpful discussions. This work was supported by the Office of Basic Energy Sciences, Office of Science, U.S. Department of Energy, under Contract No. DE-AC02-06CH11357.

[1] C. Pellegrini and S. Reiche, IEEE J. Sel. Top. Quantum Electron. **10**, 1393 (2004).
[2] J. Feldhaus, J. Arthur, and J. B. Hastings, J. Phys. B **38**, S799 (2005).
[3] J. Arthur *et al.*, Linac Coherent Light Source (LCLS) Conceptual Design Report No. SLAC-R-593 (2002) http://www-ssrl.slac.stanford.edu/lcls/cdr/
[4] *SCSS X-FEL Conceptual Design Report*, edited by Takashi Tanaka and Tsumoru Shintake (Riken, Japan, May 2005).
[5] The European X-ray Free-Electron Laser, Technical Design

Report, edited by M. Altarelli *et al.* DESY 2006-XXX (2006), http://xfel.desy.de/tdr/index_eng.html
[6] M. A. Kornberg, A. L. Godunov, S. Itza-Ortiz, D. L. Ederer, J. H. McGuire, and L. Young, J. Synchrotron Radiat. **9**, 298 (2002).
[7] *LCLS: The first experiments*, http://www-ssrl.slac.stanford.edu/lcls/papers/lcls_experiments_2.pdf
[8] H. N. Chapman *et al.*, Nat. Phys. **2**, 839 (2006).
[9] U. Saalmann and J.-M. Rost, Phys. Rev. Lett. **89**, 143401 (2002).
[10] R. Neutze, R. Wouts, D. van der Spoel, E. Weckert, and J. Hajdu, Nature (London) **406**, 752 (2000).
[11] Z. Jurek, G. Oszlanyi, and G. Faigel, Europhys. Lett. **65**, 491 (2004).
[12] G. Faigel, Z. Jurek, G. Oszlanyi, and M. Tegze, J. Alloys Compd. **401**, 86 (2005).
[13] S. P. Hau-Riege, R. A. London, G. Huldt, and H. N. Chapman, Phys. Rev. E **71**, 061919 (2005).
[14] H. Wabnitz *et al.*, Nature (London) **420**, 482 (2002).
[15] A. M. Kondratenko and E. L. Saldin, Dokl. Akad. Nauk SSSR **249**, 843 (1979) [Sov. Phys. Dokl. **24**, 986 (1979)].
[16] R. Bonifacio, C. Pellegrini, and L. M. Narducci, Opt. Commun. **50**, 373 (1984).
[17] R. Bonifacio, L. De Salvo, P. Pierini, N. Piovella, and C. Pellegrini, Phys. Rev. Lett. **73**, 70 (1994).
[18] E. L. Saldin, E. A. Schneidmiller, and M. V. Yurkov, Opt. Commun. **148**, 383 (1998).
[19] E. L. Saldin, E. A. Schneidmiller, and M. V. Yurkov, *The Physics of Free Electron Lasers* (Springer-Verlag, Berlin, 2000).
[20] S. Krinsky and R. L. Gluckstern, Phys. Rev. ST Accel. Beams **6**, 050701 (2003).
[21] LCLS parameters may be found at http://www-ssrl.slac.stanford.edu/htbin/rdbweb/LCLS_params_DB_public/
[22] The coherence time is given by $\tau=\sqrt{\pi}/\sigma_\omega$, where σ_ω is the SASE gain bandwidth [20]. Using Refs. [20,21], we estimate that the gain bandwidth at 800 eV is 0.35 eV, resulting in a coherence time of 3.3 fs.
[23] J. Andruszkow *et al.*, Phys. Rev. Lett. **85**, 3825 (2000).
[24] S. V. Milton *et al.*, Science **292**, 2037 (2001).
[25] Y. Li, J. Lewellen, Z. Huang, V. Sajaev, and S. V. Milton, Phys. Rev. Lett. **89**, 234801 (2002).
[26] Y. Li, S. Krinsky, J. W. Lewellen, K.-J. Kim, V. Sajaev, and S. V. Milton, Phys. Rev. Lett. **91**, 243602 (2003).
[27] A. Murokh *et al.*, Phys. Rev. E, **67**, 066501 (2003).
[28] V. Ayvazyan *et al.*, Phys. Rev. Lett. **88**, 104802 (2002).
[29] R. J. Glauber, Phys. Rev. **130**, 2529 (1963).
[30] R. J. Glauber, Phys. Rev. **131**, 2766 (1963).
[31] R. J. Glauber, in *Quantum Optics and Electronics*, edited by C. DeWitt (Gordon and Breach, Science Publishers, New York, 1965).
[32] L. Mandel and E. Wolf, Rev. Mod. Phys. **37**, 231 (1965).
[33] N. V. Cohan and H. F. Hameka, Phys. Rev. **151**, 1076 (1966).
[34] P. Lambropoulos, C. Kikuchi, and R. K. Osborn, Phys. Rev. **144**, 1081 (1966).
[35] M. C. Teich and G. J. Wolga, Phys. Rev. Lett. **16**, 625 (1966).
[36] S. Carusotto, G. Fornaca, and E. Polacco, Phys. Rev. **157**, 1207 (1967).
[37] Y. R. Shen, Phys. Rev. **155**, 921 (1967).
[38] P. Lambropoulos, Phys. Rev. **168**, 1418 (1968).
[39] B. R. Mollow, Phys. Rev. **175**, 1555 (1968).
[40] G. S. Agarwal, Phys. Rev. A **1**, 1445 (1970).
[41] C. Lecompte, G. Mainfray, C. Manus, and F. Sanchez, Phys. Rev. Lett. **32**, 265 (1974).
[42] C. Lecompte, G. Mainfray, C. Manus, and F. Sanchez, Phys. Rev. A **11**, 1009 (1975).
[43] D. S. Elliott, M. W. Hamilton, K. Arnett, and S. J. Smith, Phys. Rev. Lett. **53**, 439 (1984).
[44] D. S. Elliott, M. W. Hamilton, K. Arnett, and S. J. Smith, Phys. Rev. A **32**, 887 (1985).
[45] C. Chen, M. Rifani, J. Cha, Y. Y. Yin, and D. S. Elliott, Phys. Rev. A **49**, 461 (1994).
[46] J. Ducuing and N. Bloembergen, Phys. Rev. **133**, A1493 (1964).
[47] Y. Qu and S. Singh, Opt. Commun. **90**, 111 (1992).
[48] R. Santra and C. H. Greene, Phys. Rev. A **70**, 053401 (2004).
[49] H. Wabnitz, A. R. B. de Castro, P. Gürtler, T. Laarmann, W. Laasch, J. Schulz, and T. Möller, Phys. Rev. Lett. **94**, 023001 (2005).
[50] H. Friedrich, *Theoretical Atomic Physics* (Springer-Verlag, Berlin, 1994).
[51] R. Hanbury Brown and R. Q. Twiss, Nature (London) **177**, 27 (1956).
[52] E. Ikonen, Phys. Rev. Lett. **68**, 2759 (1992).
[53] M. Yabashi, K. Tamasaku, and T. Ishikawa, Phys. Rev. Lett. **88**, 244801 (2002).
[54] M. Yabashi, K. Tamasaku, and T. Ishikawa, Phys. Rev. A **69**, 023813 (2004).
[55] S. H. Southworth, E. P. Kanter, B. Krässig, L. Young, G. B. Armen, J. C. Levin, D. L. Ederer, and M. H. Chen, Phys. Rev. A **67**, 062712 (2003).
[56] L. S. Cederbaum and W. Domcke, Adv. Chem. Phys. **36**, 205 (1977).
[57] R. Loudon, *The Quantum Theory of Light* (Oxford University Press, Oxford, 1983).
[58] B. Saleh, *Photoelectron Statistics* (Springer, Berlin, 1978).
[59] V. Schmidt, *Electron Spectrometry of Atoms Using Synchrotron Radiation* (Cambridge University Press, Cambridge, England, 1997).
[60] S. A. Novikov and A. N. Hopersky, J. Phys. B **35**, L339 (2002).
[61] G. Vannucci and M. C. Teich, Appl. Opt. **19**, 548 (1980).
[62] Los Alamos National Laboratory Atomic Physics Codes, http://aphysics2.lanl.gov/cgi-bin/ION/runlanl08a.pl
[63] J. A. R. Samson, Z. X. He, L. Yin, and G. N. Haddad, J. Phys. B **27**, 887 (1994).
[64] L. R. Andersson and J. Burgdörfer, Phys. Rev. Lett. **71**, 50 (1993).
[65] J. A. R. Samson, C. H. Greene, and R. J. Bartlett, Phys. Rev. Lett. **71**, 201 (1993).
[66] J. A. R. Samson, Z. X. He, R. J. Bartlett, and M. Sagurton, Phys. Rev. Lett. **72**, 3329 (1994).
[67] R. Wehlitz, I. A. Sellin, O. Hemmers, S. B. Whitfield, P. Glans, H. Wang, D. W. Lindle, B. Langer, N. Berrah, J. Viefhaus, and U. Becker, J. Phys. B **30**, L51 (1997).
[68] K. I. Hino, P. M. Bergstrom, Jr., and J. H. Macek, Phys. Rev. Lett. **72**, 1620 (1994).
[69] J. H. McGuire, N. Berrah, R. J. Bartlett, J. A. R. Samson, J. A. Tanis, C. L. Cocke, and A. S. Schlachter, J. Phys. B **28**, 913

(1995).
[70] C. P. Bhalla, N. O. Folland, and M. A. Hein, Phys. Rev. A **8**, 649 (1973).
[71] M. O. Krause, M. L. Vestal, W. H. Johnston, and T. A. Carlson, Phys. Rev. **133**, A385 (1964).
[72] T. A. Carlson and M. O. Krause, Phys. Rev. Lett. **14**, 390 (1965).
[73] H. Bachau, J. Phys. B **17**, 1771 (1984).